Design of GaN-Based PCSEL With Temperature-Insensitive Lasing Wavelength

Qifa Liu, Zhenhai Wang, Xinyu Ma, Jin Wang, and Weidong Zhou, *Senior Member, IEEE*

***Abstract*—Considering the compensation of thermo-optic coefficients (TOC) between GaN-based cavity and TiO_2 photonic crystal (PhC) layer, we have theoretically designed a photonic crystal surface emitting laser (PCSEL) with temperature-insensitive wavelength. The structure includes a freestanding GaN membrane with embedded multiple InGaN/GaN quantum well (QW) layer and the top TiO_2 PhC layer. The high refractive index (RI) of PhC and the freestanding membrane cavity structure cooperate to enable a stronger field-coupling in PhC, thus fulfill the athermal coupling condition. Interestingly, the wavelength temperature dependence is only 0.0015 nm/°C for such PCSEL with a 82% PhC confinement factor, and its athermal property is proportional to the field confinement factor in TiO_2 PhC layer. To illustrate, a general formula has been developed after the investigations of thermo-optic effect and thermal expansion effect.**

***Index Terms*—Temperature-insensitive wavelength, PCSEL, TiO_2 photonic crystal, thermo-optic effect, thermal expansion.**

I. Introduction

SEMICONDUCTOR lasers with either bulk or quantum well (QW) active regions suffer from poor temperature stability due to self-heating and variation of the ambient temperature. For example, the lasing threshold increases and the power efficiency decreases exponentially with the increasing temperature [1]. While the stable lasing threshold and power efficiency can be realized by material designs and QW dopings [1]–[4], the lasing wavelength is still quite sensitive to the temperature. For instance, it has been proved by experiments that the wavelengths of a Fabry–Perot type GaN blue laser have linear red shifts with temperature by 0.0149 nm/°C [5]. Nevertheless, the wavelength stability is an essential feature required for semiconductor lasers. In order to maintain a good performance for semiconductor lasers, the thermoelectric cooling device is always necessary to stabilize the temperature, which also complicates the system integration. Therefore, it's desired to have a function of self-contained wavelength stability to miniature the laser modules for low-cost, small volume and flexible packaging requirement in various applications.

Several solutions have been proposed to realize wavelength stability in optical structures. One straightforward method is to employ materials with negative thermo-optic coefficient (TOC) to compensate the positive ones. For example, negative TOC materials such as liquid or polymers have been successfully used to realize stable resonant wavelength of photonic crystal (PhC) cavities [6], [7] and micro-ring resonators [8]–[10]. Such method is also feasible for designing temperature-insensitive lasers, for instance, our PCSEL design here and the vertical cavity surface emitting laser (VCSEL) reported by V. A. Shchukin *et al.* [11]. However, different from those passive components, achieving wavelength stability in lasers is more challenging and rarely reported, because of the strict lasing conditions, including the requirements of refractive index (RI), high mode quality factor and coupling strength in gain media. Another method is using temperature-insensitive bandgap material [12]–[14]. There are some reports to control the wavelength drift by using two resonances with sub-wavelength insertions of different materials [15] or tilted resonant cavity [16]. Moreover, Andrei P. Bakoz reported a kind of ambient-temperature insensitive wavelength hybrid laser [17]. This method only compensates the low ambient-temperature by tuning the laser wavelength via nonlinear absorptive heating in the laser cavity. It is necessary to ensure the wavelength stability even at high temperatures over a large range, because of the inevitable heat produced by the laser itself.

In this work we theoretically designed a GaN based wavelength-stable photonic crystal surface emitting laser. The lasing wavelength of PCSEL is a cavity feature whose resonance varies with material refractive indices. As thermo-optic coefficient for traditional semiconductor PCSEL materials are positive [18], [19], it is an effective and feasible way to select a cladding with negative TOC, to realize a stable lasing wavelength of PCSEL. Meanwhile, the proper design of the gain structure can ensure low loss mode oscillating. In our design, TiO_2 PhC layer which has negative TOC is employed as the top cladding layer in order to realize TOC compensation of the cavity. On the

Manuscript received April 9, 2021; revised June 17, 2021; accepted June 17, 2021. Date of publication June 22, 2021; date of current version July 8, 2021. This work was supported in part by the China Scholarship Council (201908320061), in part by the China Postdoctoral Science Foundation under Grant 2018M640507, and in part by the Open research fund of the National and Local Joint Engineering Laboratory of RF Integration and Micro-Assembly Technology under Grant KFJJ20180202. *(Qifa Liu and Zhenhai Wang contributed equally to this work.) (Corresponding authors: Jin Wang; Weidong Zhou.)*

Qifa Liu is with the College of Telecommunication and Information Engineering, Nanjing University of Posts and Telecommunications, Nanjing 210003, China, and also with the National and Local Joint Engineering Laboratory of RF Integration and Micro-Assembly Technology, Nanjing University of Posts and Telecommunications, Nanjing 210003, China (e-mail: liuqf@njupt.edu.cn).

Zhenhai Wang and Jin Wang are with the College of Telecommunication and Information Engineering, Nanjing University of Posts and Telecommunications, Nanjing 210003, China (e-mail: wangzh@njupt.edu.cn; jinwang@njupt.edu.cn).

Xinyu Ma is with the Department of Electrical Engineering, Tsinghua University, Beijing 100084, China (e-mail: mxy18@mails.tsinghua.edu.cn).

Weidong Zhou is with the Department of Electrical Engineering, University of Texas at Arlington, Arlington, TX 76019 USA (e-mail: wzhou@uta.edu).

Digital Object Identifier 10.1109/JPHOT.2021.3091140

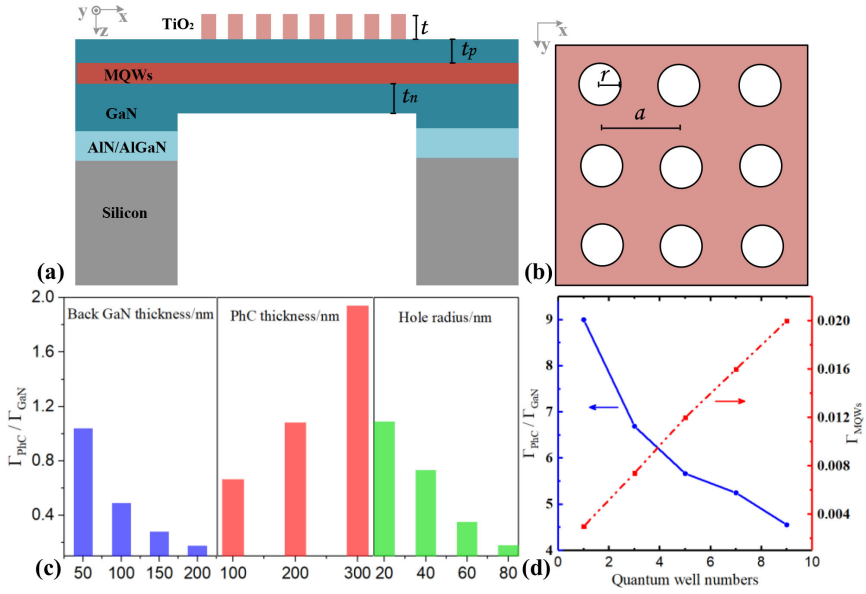

Fig. 1. (a) The configuration of the GaN membrane surface emitting laser on silicon platform combined with a TiO_2 PhC layer; (b) the top view of TiO_2 PhC square lattice layer; (c) the impact of GaN membrane back thickness (t_n), PhC layer thickness (t) and hole radius (r) influence on the confinement factors; (d) the optical field confinement factors changing with the QW numbers.

other hand, a freestanding GaN active membrane is incorporated to provide desired mode distribution strength in the PhC and active media. The freestanding membrane featured with air as the bottom cladding layer of the resonant cavity, enables high field confinement factor in TiO_2 PhC layer. Thus the negative TOC compensation effect of TiO_2 to positive TOC GaN based cavity could be promoted. Based on this configuration, the stable effective refractive index (ERI) condition and low loss mode resonance in PhC and active media are satisfied simultaneously, to realize GaN-based laser exhibiting a temperature-insensitive resonant wavelength.

II. Laser Design and Athermal Properties

In order to obtain high field coupling strength, the GaN-based active membrane with multi-quantum wells (MQWs) is combined with a top TiO_2-based PhC layer, as shown as the schematic diagram in Fig. 1(a) and (b). The laser cavity structure is composed of square lattice TiO_2 PhC layer with thickness t, lattice constant a, hole radius r, p-GaN layer with thickness t_p, n-GaN layer with thickness t_n, QW pair numbers n, a pair of QW is InGaN 3 nm / GaN 10 nm.

TiO_2 is a stable and widely used material, which has been successfully integrated in CMOS devices and micro-nano fabricated structures [20]–[23]. The RI of TiO_2 is about 2.55 around 450 nm wavelength with a negligible absorption [20]–[22]. Such high RI is beneficial to the PCSEL's design which can regulate the mode distribution and further obtain a high confinement factor in the PhC layer. More importantly, TiO_2 has a negative thermo-optic coefficient of $\sim$-3 $\times 10^{-5}$ K^{-1} at 450 nm wavelength [24], [25]. In fact, there have been reports of using TiO_2 as the RI compensation material to realize athermal silicon based micro-ring resonators [26], [27]. The proposed configuration can be fabricated through GaN-on-silicon platform. The fabrication of freestanding structure on GaN-silicon platform is a mature technology which has been widely reported in LED radiation pattern [28], [29] and enhance light extraction [30], [31]. TiO_2 micro-nano structure etching is compatible with GaN, it has been used as high contrast grating reflector in GaN-VCSELs [32]. After PhC fabrication and photoresist protection, the backside lithography aligned with the top PhC layer, is performed to guarantee the freestanding configuration. Then, back-etching is used to remove silicon substrate and thin III-V compound. In this step, all of AlN/AlGaN buffer layer and part of n-GaN layer are removed. AlN/AlGaN layer is traditionally adopted to buffer the lattice mismatch in silicon-GaN platform. By proper membrane back-thinning, the mode distribution can be effectively and conveniently controlled.

The wavelength drift induced by thermo-optic effect can be expressed as (1) [10], [26],

$$\frac{\mathrm{d}\lambda}{\mathrm{dT}} = \frac{\lambda_0}{\mathrm{N_g}} \times \frac{\mathrm{dN_{eff}}}{\mathrm{dT}} \tag{1}$$

where T is the temperature, λ_0 is the resonant wavelength, N_{eff} is the ERI of the membrane structure, N_g is the group index of the whole membrane and can be expressed as (2),

$$\mathrm{N_g} = \mathrm{N_{eff}} - \lambda_0 \times \frac{\mathrm{dN_{eff}}}{\mathrm{d\lambda}} \tag{2}$$

$\frac{\mathrm{dN_{eff}}}{\mathrm{dT}}$ is calculated by (3),

$$\frac{\mathrm{dN_{eff}}}{\mathrm{dT}} = \Gamma_{\mathrm{PhC}} \frac{\partial \mathrm{n_{TiO2}}}{\partial \mathrm{T}} + \Gamma_{\mathrm{GaN}} \frac{\partial \mathrm{n_{GaN}}}{\partial \mathrm{T}} \tag{3}$$

where Γ_{PhC} and Γ_{GaN} are the field confinement factor in TiO_2 PhC layer and GaN membrane respectively. Based on (1)–(3), the wavelength stable condition (athermal condition) is written

as (4),

$$\Gamma_{\mathrm{PhC}}\frac{\partial \mathrm{n_{TiO2}}}{\partial \mathrm{T}}+\Gamma_{\mathrm{GaN}}\frac{\partial \mathrm{n_{GaN}}}{\partial \mathrm{T}}=0 \tag{4}$$

because the thermo-optic coefficient of GaN [33], [34] is ~1.5 $\times 10^{-4}$ K^{-1}, the athermal condition for the designed PCSEL should be

$$\frac{\Gamma_{\mathrm{PhC}}}{\Gamma_{\mathrm{GaN}}}=\frac{1.5\times 10^{-4}}{3\times 10^{-5}}=5 \tag{5}$$

The field confinement factors Γ_{PhC} and Γ_{GaN}, and the gain threshold g_{th} are the most important indicators for PCSEL design. These indicators can be mainly optimized by the parameters of *t*, *a*, *r*, *n*. The confinement factors and gain threshold are calculated by using RCWA (Rigorous Coupled Wave Analysis) based Stanford Stratified Structure Solver (S4) software [35]. The gain threshold is derived from (6),

$$\mathrm{g_{th}}=\frac{\alpha}{\Gamma_{\mathrm{QW}}} \tag{6}$$

where α is the vertical radiation loss, Γ_{QW} is the field confinement factor in MQWs. For PCSEL device with large PhC area (for instance >400 μm length), the in-plane loss and the internal loss are negligible [36]–[38], so only the vertical radiation loss is considered and calculated by (7),

$$\alpha=\frac{2\pi}{\mathrm{Q}\cdot \mathrm{a}} \tag{7}$$

where *a* is the lattice constant, *Q* is the quality factor obtained by Fano fitting the guided resonances in reflection spectra. The confinement factors in MQWs and PhCs can be calculated by (8).

$$\Gamma_{\mathrm{QW}}=\frac{\int_{\mathrm{QW}}(\mathrm{E_x^2}+\mathrm{E_y^2})\cdot \mathrm{dv}}{\int_{\mathrm{cav}}(\mathrm{E_x^2}+\mathrm{E_y^2})\cdot \mathrm{dv}},\ \Gamma_{\mathrm{PhC}}=\frac{\int_{\mathrm{PhC}}(\mathrm{E_x^2}+\mathrm{E_y^2})\cdot \mathrm{dv}}{\int_{\mathrm{cav}}(\mathrm{E_x^2}+\mathrm{E_y^2})\cdot \mathrm{dv}} \tag{8}$$

In S4 simulations, bottom and top air thicknesses are set to be infinite. Transverse electric (TE) waves are considered, and the RI at room temperature are as follows: $n_{air}=1$, $n_{GaN}=2.39$, $n_{InGaN}=2.46$, $n_{TiO2}=2.55$.

The laser configurations with different parameters are investigated at first. The distance between PhC and MQWs, as well as the membrane thickness, is crucial to the field distribution intensity. The smaller top/bottom GaN thickness means the shorter distance between PhC and active layer, and the higher field intensity, corresponding to a high confinement factor in PhC region. In order to acquire higher Γ_{PhC}, there should be a small distance between PhC and MQWs, as well as thinner membrane. The smaller t_n and t_p are beneficial to a stronger field coupling in PhC. On the other hand, the higher ERI can shift the field concentration towards the PhC layer, which are contributed to a larger PhC thickness and a smaller hole radius. As shown in Fig. 1(c), the higher $\Gamma_{PhC}/\Gamma_{GaN}$ value is corresponding to t = 300 nm PhC thickness and $r = 20$ nm hole radius. Besides, the resonance in PhC cavity with $r = 20$ nm has higher quality factor which is crucial to demonstrate small threshold gain of laser. The above parameters combine together can give birth to much higher values of $\Gamma_{PhC}/\Gamma_{GaN}$.

TABLE 1
LIST OF PARAMETERS AND PERFORMANCES OF THE OPTIMIZED ATHERMAL PCSEL AND THE COMPARED PCSEL

Case A (optimized)	Case B (compared)
n = 9	n = 7
t = 300 nm	t = 200 nm
r = 20 nm	r = 40 nm
t_p = 50 nm	t_p = 50 nm
t_n = 50 nm	t_n = 200 nm
a =184 nm	a = 196 nm
Γ_{PhC} = 82%	Γ_{PhC} = 8.4%
$\Gamma_{PhC}/\Gamma_{GaN}$ = 4.6	$\Gamma_{PhC}/\Gamma_{GaN}$ = 0.1

Some parameters for a higher Γ_{PhC} are contrary to the lower threshold gain g_{th}. For instance, the smaller membrane thickness is corresponding to the higher Γ_{PhC} but the larger cavity loss. As shown in (6), the higher confinement factor in MQWs is an essential condition for the low-threshold lasing. MQWs design can be used as a conflict resolving method to promote Γ_{QW} for the lower threshold gain while maintaining a high Γ_{PhC}. Because the InGaN QW layer with higher RI pushes field profile more into GaN membrane, there is still a trade-off for higher Γ_{QW} and Γ_{PhC}. QW numbers were investigated by fixing parameters of t_n, t_p, r, t. As shown in Fig. 1(d), $\Gamma_{PhC}/\Gamma_{GaN}$ and Γ_{QW} changed linearly with different QW numbers at t = 300 nm, $r = 20$ nm, $t_p = 50$ nm, $t_n = 50$ nm. A large QW number helps to promote confinement factor in gain media to achieve high oscillation gain. QW numbers will not affect the propagation loss a lot, if the total loss is dominated by the vertical scattering in large PhC area design. When the QW numbers reach 7 pairs or more, Γ_{QW} increases to more than 0.016 and g_{th} can be as small as around 1000 cm^{-1}. In this situation, the $\Gamma_{PhC}/\Gamma_{GaN}$ value can still be reached about 5 due to the 300 nm thick TiO_2 PhC layer with high ERI. This explains the reason why use such a thick PhC layer, small hole radius and thin GaN in the optimized design, because we should also consider the laser gain threshold when getting high Γ_{PhC}. We use more QW numbers to promote Γ_{QW} to decrease g_{th}. On the other hand, more InGaN well layers with higher RI can pull field profile more into GaN membrane which makes Γ_{PhC} smaller. It should be noticed that, larger QW numbers bring higher voltage drop. The effect of the non-uniformity of the carrier distribution with too large QW number degrades the lasing characteristics, and limits the output power.

Table 1 gives the parameters and performance list of the optimized PCSEL named as Case A and the compared one as Case B. Case B is with $\Gamma_{\mathrm{PhC}} = 8.4\%$ which is in the typical confinement factor value range for PCSELs without considering wavelength stability. Case A adopts 9 QW numbers combined with the optimized parameters. Compared with Case B with $\Gamma_{PhC}/\Gamma_{GaN} = 0.1$, the gain threshold of Case A can below 1000 cm^{-1} while $\Gamma_{PhC}/\Gamma_{GaN}$ value can still reach 4.6. The variable lattice constant a can tune the laser wavelength. In A and B cases here, we have adopted 184 nm and 196 nm in

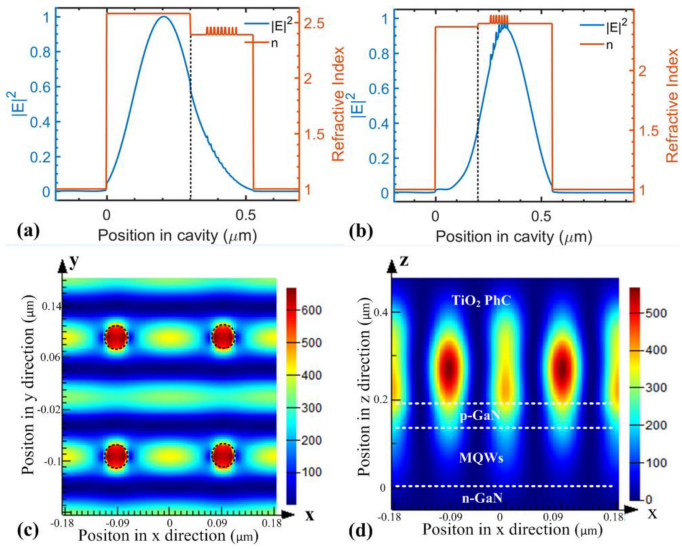

Fig. 2. Mode profile in (a) the optimized laser cavity (Case A) and (b) the compared laser cavity (Case B); FDTD simulated (c) x-y plane field distribution in the PhC layer and (d) x-z plane field distribution of the optimized PCSEL.

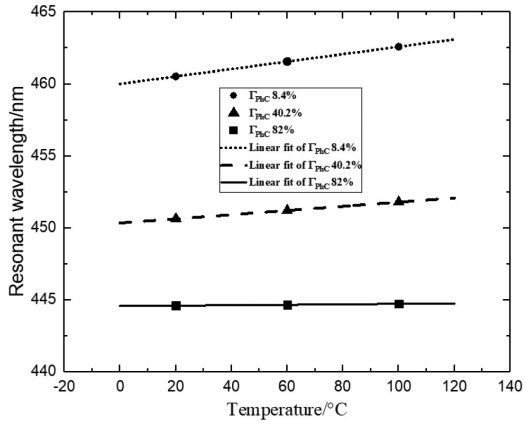

Fig. 3. The resonant wavelength drifts under variable temperatures for different PCSELs: $\Gamma_{PhC} = 8.4\%$, $n = 7$, $t = 200$ nm, $r = 40$ nm, $t_p = 50$ nm, $t_n = 200$ nm, $a = 196$ nm;$\Gamma_{PhC} = 40.2\%$, $n = 1$, $t = 100$ nm, $r = 40$ nm, $t_p = 50$ nm, $t_n = 50$ nm, $a = 200$ nm; $\Gamma_{PhC} = 82\%$, $n = 9$, $t = 300$ nm, $r = 20$ nm, $t_p = 50$ nm, $t_n = 50$ nm, $a = 184$ nm.

order to have resonant wavelengths in the 430∼450 nm active media wavelength range. Correspondingly, Fig. 2(a), (c), and (d) exhibit field profile and distribution of Case A, while Fig. 2(b) exhibits field distribution of Case B for comparison. As shown in Fig. 2(a) and (b), both of the two structures form fundamental modes in the resonant cavities, which are calculated by RCWA. Fig. 2(c) and (d) are the x-y plane distributions and x-z plane distributions in the PhC layer simulated by finite difference time domain (FDTD) method. The FDTD models are calculated with a spatial grid of *a/64*, the PhC area is infinite in xy direction, light source is TE mode plane wave, RI of different layers are the same as those in above S4 simulations. For the optimized PCSEL (Case A), both RCWA and FDTD results have shown that the fundamental mode field is largely confined in the PhC layer. Thanks to the high RI of TiO_2 PhC layer and the membrane design of the waveguide-like structure with a small distance between PhC and active region, we could obtain a stronger coupling strength of fundamental mode confined in PhCs. It should be noted that, Case A has a lower mode overlap in the gain medium, which may means more heating due to higher pumping needed for lasing. Nevertheless, this optimized PCSEL design can fulfill wavelength stable function and has general laser properties.

PCSEL utilizes multidirectional distributed feedback (DFB) effect near the band edges in PhCs. The coupling in two-dimensional PhCs provides mode oscillating behavior and extracts light vertically. The lasing wavelength is characterized as the resonant reflected peaks of GaN membrane with TiO_2 PhCs. The temperature insensitive properties of the PCSEL have been explored by S4 simulation. The RI at different temperatures are set accordingly to the TOC value of TiO_2 and GaN. Fig. 3 exhibits relations between lasing wavelength and temperature in different PCSEL configurations. Resonances of $\Gamma_{PhC} = 8.4\%$ and $\Gamma_{PhC} = 40.2\%$ show obvious resonant wavelengths drift with 0.026 nm/°C and 0.015 nm/°C, respectively. The optimized PCSEL configuration with $\Gamma_{PhC} = 82\%$ remains exceptionally stable wavelength at 444.6 nm, with a gradient of only 0.0015 nm/°C. This represents a dramatic reduction in temperature dependence of the designed PCSEL according to the athermal condition of (3). Fig. 4(a)(b) shows the resonant spectrum for the configurations with $\Gamma_{PhC} = 8.4\%$ and $\Gamma_{PhC} = 82\%$ under different ambient temperatures. It is clear that, the optimized PCSEL has only a tiny wavelength shift which is primarily attributed to the small difference of $\Gamma_{PhC}/\Gamma_{GaN} = 4.6$ compared to the athermal condition $\Gamma_{PhC}/\Gamma_{GaN} = 5$.

Except for the thermo-optical effect, the thermal expansion effect can also influence the drift of the resonant frequency in PCSEL with variable temperatures. In the following discussion, we have only considered the TiO_2 thermal expansion effect on lattice constant regardless of the small effect on the wavelength from the PhC layer thickness and hole radius. The thermal expansion effect on lattice constant a is $\mathrm{d}a/\mathrm{d}T = a_0 \times \alpha_{TiO2} = a_0 \times 8.4\times10^{-6}$. Meantime, $\mathrm{d}\lambda/\mathrm{d}a = 2.3$ can be obtained by simulations in the designed PCSEL. Thus, thermal expansion effect on the wavelength drift can be expressed as (9),

$$\frac{\mathrm{d}\lambda}{\mathrm{dT}} = 2.3 \times 8.4 \times 10^{-6} \times \mathrm{a}_0 = 1.9 \times 10^{-5} \times \mathrm{a}_0 \qquad (9)$$

Combine (1)–(3) with (9), the general formula of wavelength drift induced by thermo-optic effect and thermal expansion effect can be expressed as (10),

$$\frac{\mathrm{d}\lambda}{\mathrm{dT}} = \frac{\lambda_0}{\mathrm{N_{eff}} - \lambda_0 \times \frac{\mathrm{dN_{eff}}}{\mathrm{d}\lambda}} \left(-3\times10^{-5}\Gamma_{\mathrm{PhC}} + 1.5\times10^{-4}\Gamma_{\mathrm{GaN}} \right) + 1.9 \times 10^{-5} \times \mathrm{a}_0 \qquad (10)$$

where λ_0 is the resonant wavelength, a_0 is the corresponding lattice constant. N_{eff} at different wavelength can be calculated for the optimized PCSEL structure where $\Gamma_{PhC} = 82\%$, $\Gamma_{GaN} = 18\%$, $\lambda_0 = 444.61$ nm, $a_0 = 184$ nm, $\mathrm{N_{eff}} = 2.42$. $\mathrm{dN_{eff}}/\mathrm{d}\lambda = -3\times10^{-4}$ can be derived from our N_{eff} calculations based on RCWA. By using (10), we calculate the wavelength drift which is mainly manipulated by the thermal expansion effect. For the compared PCSEL with $\Gamma_{\mathrm{PhC}} = 8.4\%$, the calculated wavelength drift is mainly induced by thermo-optic effect.

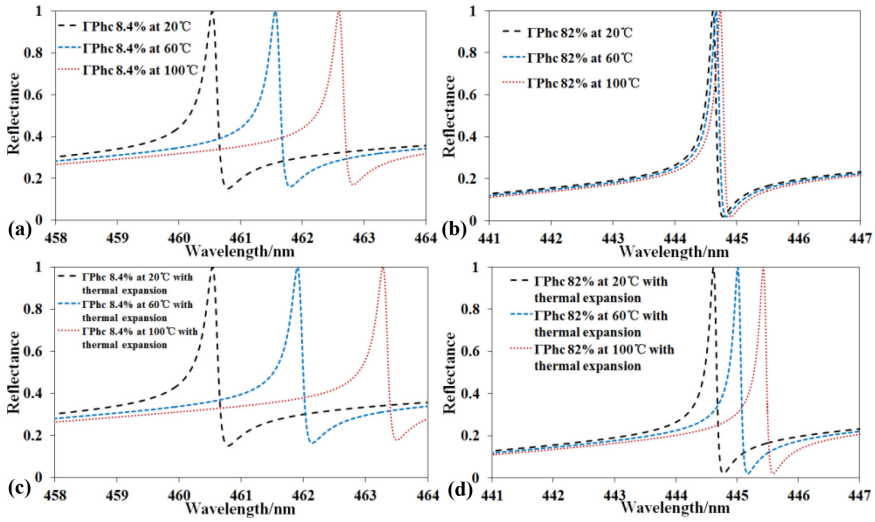

Fig. 4. Normalized reflectance spectra of lasers in (a)(c) $\Gamma_{PhC} = 8.4\%$ (Case B) and (b)(d) $\Gamma_{PhC} = 82\%$ (Case A) as a function of temperature. (a)(b) Consider thermo-optic effect only, (c)(d) Consider both thermo-optic effect and thermal expansion effect.

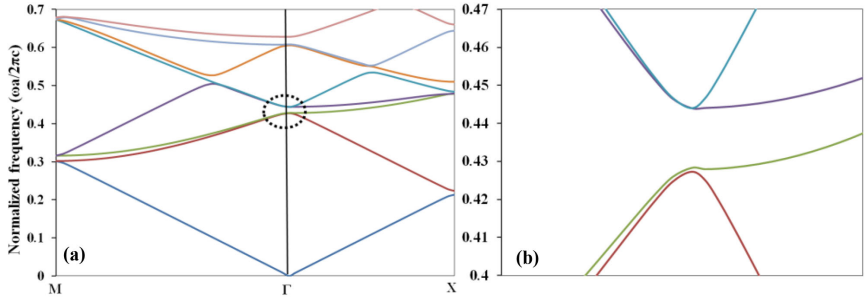

Fig. 5. (a) The photonic band structures of the optimized temperature-insensitive PCSEL of TE polarization and (b) the enlarged view of the band gap and edges at the Γ point.

Fig. 4(c)(d) shows the wavelength drift induced by thermo-optic effect and thermal expansion mutually. Compared to the Fig. 4(a)(b), a larger wavelength shift is observed. These results agree well with theoretical analysis, that thermo-optic effect and thermal expansion manipulate wavelength drift for PCSEL with $\Gamma_{\mathrm{PhC}} = 8.4\%$ and $\Gamma_{\mathrm{PhC}} = 82\%$, respectively.

In order to further verify our laser design, the photonic band structures of Case A was calculated by MIT photonic bands (MPB) [39], based on fully vectoral plane wave expansion method (PWE). The general calculation approach can be referred in some other reports [40], [41]. The designed laser works at the band edge of the denoted Γ point in Fig. 5(a). Fig. 5(b) shows the enlarged view of the band gap and edges at the Γ point. When a wavelength is equal to the lattice constant condition, for instance in one Γ–X direction, it is diffracted not only backward, but also in other equivalent Γ–X directions. The wavelets scattered are in-phase so standing wave is formed at Γ point in the 2D photonic crystal. A lasing oscillation is considered to occur at either of the band edges of the Γ point, and the lasing action occurs at the mode with the lowest gain threshold. All the other modes are also possible to lase with sufficient pump power. We consider the laser wavelength at 440 nm, lattice constant is 184 nm, the normalized frequency of the emission of the present structure is around 0.42. This value is in accordance with the denoted Γ point position in the band diagram.

When we consider the real device, it will be affected by various factors, for instance, the TOC of TiO_2 will change with the growth conditions such as the chamber pressure, and the quality and aperture of PhCs are restricted by the micro nano fabrication accuracy. The common method used to realize PhC structure is electron beam lithography (EBL), which still has obstacles to realize 20 nm hole radius especially for thick layers. Focused ion beam (FIB) is an alternative choice to realize PhC with small holes, whose resolution can be around 10 nm. The hole profile is another problem for PhC laser design. The shape of PhC will influence the Q factor of resonance and may bring degradation of laser performance. Therefore, this design needs to combine with the actual fabrication process and accurate materials growth. If so, the $\Gamma_{PhC}/\Gamma_{GaN}$ can be optimized to achieve the optimal temperature insensitive characteristics of lasing wavelength. By the way, current injection is also a common problem for GaN based lasers because of the low carrier mobility of p-GaN. For our proposed laser with insulating TiO_2 PhC layer, the current injection problem can be solved by such following ways: (1) designing the position and shape of p/n electrodes in order to form uniform and efficient carrier injection in active media, (2) introducing ITO conductive layer under the PhC layer, (3) controlling the doping concentration of p/n GaN, such as reducing the resistance of p-GaN and increasing the resistance of n-GaN.

III. Conclusion

In conclusion, we have theoretically proposed a temperature-insensitive GaN-based PCSEL and investigated its thermal drift of the resonant frequency caused by thermo-optic and thermal expansion effects. The confinement factor, gain threshold, field distribution, resonant wavelength temperature-dependent properties were investigated by RCWA, FDTD simulation and theoretical analysis. Thermo-optic stabilization can be achieved by forming a laser cavity with suitable configuration and dimensions. A general principle and design method has been introduced for temperature-insensitive PCSEL. Although, the proposed membrane configuration may suffer high thermal resistance problem, it is the design of photonic crystal surface emitting lasers with enhancing laser-wavelength stability under variable temperatures caused by self-heating or other external environments.

References

[1] Y. Bai, N. Bandyopadhyay, S. Tsao, E. Selcuk, S. Slivken, and M. Razeghi, "Highly temperature insensitive quantum cascade lasers," *Appl. Phys. Lett.*, vol. 97, no. 25, 2010, Art. no. 251104.

[2] L. V. Asryan and S. Luryi, "Temperature-insensitive semiconductor quantum dot laser," *Solid State Electron.*, vol. 47, no. 2, pp. 205–212, 2003.

[3] O. B. Shchekin and D. G. Deppe, "The role of p-type doping and the density of states on the modulation response of quantum dot lasers," *Appl. Phys. Lett.*, vol. 80, no. 15. pp. 2758–2760, 2002.

[4] S. Mikhrin *et al.*, "High power temperature-insensitive 1.3 μm InAs/InGaAs/GaAs quantum dot lasers," *Semicond. Sci. Technol.*, vol. 20, no. 5 pp. 340–342, 2005.

[5] W. Al-Basheer, T. O. Adigun, A. Aljalal, and K. Gasmi, "Spectral and spatial dynamics of a multimode GaN-based blue laser diode," *J. Mod. Optic.*, vol. 67, no. 4, pp. 355–360, 2020.

[6] C. Karnutsch *et al.*, "Temperature stabilization of optofluidic photonic crystal cavities," *Appl. Phys. Lett.*, vol. 94, no. 100, 2009, Art. no. 231114.

[7] Y. Zhang and Y. Shi, "Temperature insensitive lower-index-mode photonic crystal nanobeam cavity," *Opt. Lett.*, vol. 40, no. 2, pp. 264–267, 2015.

[8] M. Han and A. Wang, "Temperature compensation of optical microresonators using a surface layer with negative thermo-optic coefficient," *Opt. Lett.*, vol. 32, no. 13, pp. 1800–1802, 2007.

[9] J.-M. Lee, D.-J. Kim, G.-H. Kim, O.-K. Kwon, K.-J. Kim, and G. Kim, "Controlling temperature dependence of silicon waveguide using slot structure," *Opt. Exp.*, vol. 16, no. 3, pp. 1645–1652, 2008.

[10] J. Teng *et al.*, "Athermal Silicon-on-insulator ring resonators by overlaying a polymer cladding on narrowed waveguides," *Opt. Exp.*, vol. 17, no. 17, pp. 14627–14633, 2009.

[11] V. A. Shchukin *et al.*, "Passive cavity surface–emitting lasers: Option of temperature–insensitive lasing wavelength for uncooled dense wavelength division multiplexing systems," *Proc. SPIE*, vol. 9766, 2016, Art. no. 976609.

[12] S. Shutts, P. M. Smowton, and A. B. Krysa, "InP quantum dot lasers with temperature insensitive operating wavelength," *Appl. Phys. Lett.*, vol. 103, 2013, Art. no. 061106.

[13] K. Oe, and H. Asai, "Proposal on a temperature-insensitive wavelength semiconductor laser," *IEICE Trans. Electron.*, vol. E79C, no. 12, pp. 1751–1759, 1996.

[14] H. Asahi, K. Yamamoto, K. Iwata, S. Gonda, and K. Oe. "New III–V compound semiconductors TlInGaP for 0.9 μm to over 10 μm wavelength range laser diodes and their first successful growth," *Jpn. J. Appl. Phys.*, vol. 35, no. 7B, pp. L876, 1996.

[15] M. B. Lifshits, V. A. Shchukin, N. N. Ledentsov, and D. Bimberg, "Resonance wavelength in planar multilayer waveguides: Control and complete suppression of temperature sensitivity," *Semicond. Sci. Technol.*, vol. 22, pp. 380–384, 2007.

[16] N. N. Ledentsov *et al.*, "Wavelength-stabilized tilted cavity quantum dot laser," *Semicond. Sci. Technol*, vol. 19, pp. 1183–1188, 2004.

[17] A. P. Bakoz *et al.*, "Wavelength stability in a hybrid photonic crystal laser through controlled nonlinear absorptive heating in the reflector," *Light-Sci. Appl.*, vol. 7, no. 39, pp. 1–7, 2018.

[18] F. G. Della Corte, G. Cocorullo, M. Iodice, and I. Rendina, "Temperature dependence of the thermo-optic coefficient of InP, gaas, and SiC from room temperature to 600 k at the wavelength of 1.5 μm," *Appl. Phys. Lett.*, vol. 77, no. 11, 2000, Art. no. 1614.

[19] C. Karnutsch *et al.*, "Temperature stabilization of optofluidic photonic crystal cavities," *Appl. Phys. Lett.*, vol. 94, no. 100, 2009, pp. 231114.

[20] E. Hashemi, J. Bengtsson, J. S. Gustavsson, S. Carlsson, G. Rossbach, and Å. Haglund, "TiO_2 membrane high-contrast grating reflectors for vertical-cavity light-emitters in the visible wavelength regime," *J. Vac. Sci. Technol. B*, vol. 33, no. 5, 2015, Art. no. 050603.

[21] J. Heo, W. Guo, and P. Bhattacharya, "Monolithic single GaN nanowire laser with photonic crystal microcavity on silicon," *Appl. Phys. Lett.*, vol. 98, no. 2, 2011, Art. no. 021110.

[22] J. Lee, J. Park, and M. Lee, "Nanostructured TiO_2 diffraction grating fabricated via imprinting and $TiCl_4$ treatment," *J. Mater. Chem. C*, vol. 2, no. 6, pp. 981–985, 2014.

[23] K.-R. Choi, J.-C. Woo, Y.-H. Joo, Y.-S. Chun, and C.-I. Kim, "Dry etching properties of TiO_2 thin films in O_2/CF_4/Ar plasma," *Vacuum*, vol. 92, pp. 85–89, 2013.

[24] M. R. Saleem, S. Honkanen, and J. Turunen, "Thermal properties of TiO_2 films fabricated by atomic layer deposition," *IOP Conf. Ser.: Mater. Sci. Eng.*, vol. 60, 2014, Art. no. 012008.

[25] S. Wiechmann and J. Müller, "Thermo-optic properties of TiO_2, Ta_2O_5 and Al_2O_3 thin films for integrated optics on silicon," *Thin Solid Films*, vol. 517, no. 24, pp. 6847–6849, 2009.

[26] B. Guha, J. Cardenas, and M. Lipson, "Athermal silicon microring resonators with titanium oxide cladding," *Opt. Exp.*, vol. 21, no. 22, pp. 26557–26562, 2013.

[27] S. S. Djordjevic *et al.*, "CMOS-compatible, athermal silicon ring modulators clad with titanium dioxide," *Opt. Exp.*, vol. 21, no. 12, pp. 13958–13968, 2013.

[28] X. Li *et al.*, "Thickness-dependent performance of a free-standing membrane LED," *IEEE Photon. J.*, vol. 7, no. 3, 2015, Art. no. 1600607.

[29] T. Wei *et al.*, "Efficiency enhancement of homoepitaxial InGaN/GaN light-emitting diodes on freestanding GaN substrate with double embedded SiO_2 photonic crystals," *Opt. Exp.*, vol. 22, no. S4, pp. A1093–A1100, 2014.

[30] X. Li, Z. Shi, G. Zhu, M. Zhang, H. Zhu, and Y. Wang, "High efficiency membrane light emitting diode fabricated by back wafer thinning technique," *Appl. Phys. Lett.*, vol. 105, 2014, Art. no. 031109.

[31] M. Wakui, H. Sameshima, F. R. Hu, and K. Hane, "Fabrication of GaN light emitting diode membrane on si substrate for MEMS applications," *Microsyst. Technol.*, vol. 17, pp. 109–114, 2011.

[32] T.-C. Chang *et al.*, "Electrically injected GaN-based vertical-cavity surface-emitting lasers with TiO_2 high-index-contrast grating reflectors," *ACS Photon.*, vol. 7, no. 4, pp. 861–866, 2020.

[33] N. Watanabe, T. Kimoto, and J. Suda, "Thermo-optic coefficients of 4H-SiC, GaN, and AlN for ultraviolet to infrared regions up to 500 °C ," *Jpn. J. Appl. Phys.*, vol. 51, no. 11R, 2012, Art. no. 112101.

[34] N. Watanabe, T. Kimoto, and J. Suda, "The temperature dependence of the refractive indices of GaN and AlN from room temperature up to 515 °C," *J. Appl. Phys.*, vol. 104, no. 10, 2008, Art. no. 106101.

[35] V. Liu and S. Fan, "S4: A free electromagnetic solver for layered periodic structures," *Comput. Phys. Commun.*, vol. 183, no. 10, pp. 2233–2244, 2012.

[36] K. Hirose, Y. Liang, Y. Kurosaka, A. Watanabe, T. Sugiyama, and S. Noda, "Watt-class high-power, high-beam-quality photonic-crystal lasers," *Nat. Photon.*, vol. 8, pp. 406–411, 2014.

[37] Y. Liang, C. Peng, K. Sakai, S. Iwahashi, and S. Noda, "Three-dimensional coupled-wave analysis for square-lattice photonic crystal surface emitting lasers with transverse-electric polarization: Finite-size effects," *Opt. Exp.*, vol. 20, no. 14, pp. 15945–15961, 2012.

[38] Z. Wang *et al.*, "Large area photonic crystal quantum cascade laser with 5 w surface-emitting power," *Opt. Exp.*, vol. 27, no. 16, pp. 22708–22716, 2019.

[39] S. G. Johnson and J. D. Joannopoulos, "Block-iterative frequency-domain methods for Maxwell's equations in a planewave basis," *Opt. Exp.*, vol. 8, no. 3, pp. 173–190, 2001.

[40] K. Sakai, E. Miyai, T. Sakaguchi, D. Ohnishi, T. Okano, and S. Noda, "Lasing band-edge identification for a surface-emitting photonic crystal laser," *IEEE J. Sel. Area Commun.*, vol. 23, no. 7, pp. 1335–1340, 2005.

[41] S. W. Chen, T. C. Lu, and T. T. Kao, "Study of GaN-based photonic crystal surface-emitting lasers (PCSELs) with AlN/GaN distributed Bragg reflectors," *IEEE J. Sel. Topics Quantum Electron.*, vol. 15, no. 3, pp. 885–891, 2009.